Geobios xxx (xxxx) xxx

Contents lists available at ScienceDirect

Geobios

journal homepage: www.elsevier.com/locate/geobio

Research Paper

Evaluation of the main drivers of environmental and climatic changes of the sea-surface across the Cretaceous-Paleogene transition: A global perspective ☆

Vicente Gilabert [a,b,*], Sietske J. Batenburg [a,d], José A. Arz [b], Nils B. Baumann [c], Marcel Regelous [c], Ignacio Arenillas [b]

[a] Departament de Dinàmica de la Terra i de l'Oceà, Facultat de Ciències de la Terra de la Universitat de Barcelona, 08028, Barcelona, Spain
[b] Departamento de Ciencias de la Tierra, and Instituto Universitario de Investigación en Ciencias Ambientales de Aragón (IUCA), Universidad de Zaragoza, E-50009 Zaragoza, Spain
[c] GeoZentrum Nordbayern, Friedrich-Alexander-Universität Erlangen-Nürnberg, Schlossgarten 5, 91054 Erlangen, Germany
[d] Department of Earth Sciences, Faculty of Geosciences, Utrecht University, Princetonlaan 8a, 3584 CB Utrecht, the Netherlands

ARTICLE INFO

Article history:
Received 27 November 2023
Revised 5 July 2024
Accepted 5 August 2024
Available online xxxx

Keywords:
Chicxulub impact
Deccan volcanism
Planktic foraminifera
Mercury
Stable isotopes

ABSTRACT

The Chicxulub impact and Deccan volcanism have long been considered opposing factors to explain the changes observed across the Cretaceous/Paleogene boundary (KPB). Although the geologically instantaneous effects of the Chicxulub impact better explain the KPB catastrophic mass extinction, refinement of geochemical and micropaleontological proxies contributes to assessing the actual role of the Deccan volcanism in environmental changes across the KPB. Furthermore, cyclostratigraphy is being used to evaluate the role of orbital forcing on climate, and to refine age models. In this paper, we evaluate the climate and environmental changes across the KPB (66.100–65.350 Ma) from a global perspective, exploring several proxies from the Pacific, Atlantic and Tethyan realms: bulk $\delta^{18}O$ and $\delta^{13}C$ disturbances, mercury enrichments, and blooms of triserial guembelitriids and aberrant planktic foraminifera. The KPB, Dan-C2 and LC29n events, dated at 66.0, 65.8–65.7 and 65.47–65.41 Ma, respectively, have been recognized in all Tethyan and Atlantic localities, but only the KPB in the Pacific. Multiproxy analysis suggests that volcanic activity of the Deccan Traps did not have a relevant role in the aforementioned events, but contributed to environmental stress in the first 10 kyr of the Danian, and between ~70 and 200 kyr after the KPB.

1. Introduction

The Cretaceous/Paleogene boundary (KPB, ~66 Ma) is recognized as one of the big five mass extinctions events, being especially catastrophic for calcareous plankton, with an extinction rate of >90% for planktic foraminifera (Arenillas et al., 2022). The planktic foraminiferal turnover across the KPB was contemporaneous with two major geological events: the emplacement of the massive (1.1×10^6 km^3) Deccan Traps large igneous province (LIP) in India (Sprain et al., 2019; Schoene et al., 2019) and the asteroid impact at Chicxulub, Mexico (Schulte et al., 2010). For decades, the untangling of climatic and environmental effects on biota caused by each event have fueled an ongoing debate among the scientific community (Li and Keller, 1998; Keller, 2008; Schulte et al., 2010; Renne et al., 2015; Keller et al., 2020; Gilabert et al., 2022). The Deccan volcanism and the Chicxulub impact operated on very different time scales, with the Deccan Traps eruptions starting 300–400 kyr prior the KPB and ending ~700 kyr later (Sprain et al., 2019; Schoene et al., 2019), while the Chicxulub impact was a geologically instantaneous event (Schulte et al., 2010; Renne et al., 2013) with its climatic and environmental perturbations occurring on a scale from days to a few kyr (Henehan et al., 2019).

It is established that the small-volume eruptive formations of the Deccan Traps ~100–250 kyr before the KPB were coincident with a transient warming episode known as the Late Maastrichtian Warming event (Li and Keller, 1998; Barnet et al., 2018), although the contribution of orbital forcing to this event may also have been significant (Gilabert et al., 2022). However, the influence of Deccan volcanism on climate during the last 100 kyr of the Maastrichtian is still highly debated (Hull et al., 2020). Despite the recent high-precision radiometric dating of the largest Deccan lava formations,

☆ Corresponding editor: Alba Sánchez-García.

* Corresponding author.
E-mail addresses: vgilabert@ub.edu, vgilabert@unizar.es (V. Gilabert).

https://doi.org/10.1016/j.geobios.2024.08.011
0016-6995/

the uncertainties on these age determinations have significant implications. According to $^{40}Ar/^{39}Ar$ dating, the large-volume Poladpur and Ambenali formations were early Danian in age and eruption may have been triggered by the Chicxulub impact (Richards et al., 2015; Renne et al., 2015). However, U-Pb zircon dating suggests that the Poladpur Fm. was erupted between ~80–30 kyr prior to the KPB (Schoene et al., 2019). Therefore, further investigation is needed to evaluate the sequence of events during the last 100 kyr of the Maastrichtian and the subsequent KPB mass extinction event. For this interval, very different interpretations are discussed among the scientific community; e.g., environmental and evolutionary stability until the Chicxulub impact (Schulte et al., 2010; Gilabert et al., 2021a), strong perturbation of the ecosystems by Deccan volcanism prior to the asteroid impact (Keller, 2008; Keller et al., 2020), or even mitigation of the latest Maastrichtian cooling due to volcanogenic greenhouse gasses (Hull et al., 2020).

High-resolution multiproxy studies of the first 700 kyr of the Danian are sparse (Quillévéré et al., 2008; Coccioni et al., 2010), but recently this time interval is receiving more attention (Barnet et al., 2019; Hull et al., 2020; Gilabert et al., 2021a, 2021b, 2022; Krahl et al., 2023; Jouini et al., 2023). It has been proposed that climatic perturbations during the early Danian, such as the Dan-C2 and the Lower Chron C29n (LC29n) events may be related to the Deccan Traps magmatism (Coccioni et al., 2010; Krahl et al., 2020). However, other authors have argued that estimations of volcanogenic CO_2 emissions, further hindered by dating uncertainties, are insufficient to establish a direct cause-effect relationship between these events and the Deccan volcanism (Barnet et al., 2019; Fendley et al., 2020), while orbital forcing may have played a significant role (Barnet et al., 2019; Gilabert et al., 2022).

For the early Danian, even small uncertainties in radiometric dating have large implications for the interpretation of climatic perturbations, as mentioned above. Therefore, to assess the role of the Deccan volcanism in climate and environmental changes across the KPB, a direct and reliable geochemical proxy of volcanic emissions is required. Mercury (Hg) enrichments in sedimentary rocks potentially meet this requirement (Percival et al., 2018; Grasby et al., 2019). While Hg anomalies yield promising results (Font et al., 2022; Keller et al., 2020), a multi-proxy approach is required to evaluate factors that may affect the reliability of the Hg signal such as changes in Hg source, organic matter deposition or redox conditions (Grasby et al., 2019).

In this study we compiled existing data and generated new micropaleontological and geochemical datasets across the KPB in some of the most continuous and expanded sections. The geographic distribution of the chosen localities (Pacific, Atlantic and Tethys) allows us to establish a global picture of climate change during this time interval. The high-resolution datasets presented here allow us to examine the paleoclimatic and paleoenvironmental changes in the surface ocean during the last 100 kyr of the Maastrichtian and the first 700 kyr of the Danian. We evaluate the different proposed Deccan eruptive models using a compilation of climate-sensitive records and compare them with potential direct evidence of volcanism (Hg anomalies) as well as with the astronomical solution, considering that orbital forcing influences global climate change. Moreover, we combine these geochemical data with planktic foraminifera from these localities in order to identify blooms of opportunistic triserial guembelitriids and aberrant specimens across the KPB, which are considered the most common indicators of high environmental stress (Arenillas et al., 2018). This new compilation of planktic foraminiferal and geochemical data allow us to identify the mechanisms that led to the ecological deterioration and/or recuperation of the sea-surface, and to evaluate the temporal relationships of biotic changes with Deccan volcanism and the KPB, Dan-C2 and LC29n events.

2. Material and methods

Here we have generated, compiled and integrated the records of three main proxies: bulk rock carbon and oxygen stable isotope ratios, planktic foraminiferal quantitative analyses and mercury/TOC anomalies, with all of them displayed on independent age models. These records come from some of the most complete and internationally recognized KPB localities worldwide including both deep sea sites and inland sections. The deep-sea sites analyzed are Ocean Drilling Program (ODP) Site 1262 and Deep-Sea Drilling Program (DSDP) Site 525 on the Walvis Ridge, South Atlantic; ODP-1209 and DSDP Site 577 on Shatsky Rise, North Pacific; and ODP-1049 at Blake Nose, North Atlantic. Land-based shallow marine localities include Zumaia and Caravaca, Spain; Bidart, France; Gubbio, Italy; and El Kef, Elles and Aïn Settara, Tunisia (Fig. 1).

2.1. Bulk stable isotope data

We generated new bulk isotope data from the El Kef ($\delta^{13}C$, $\delta^{18}O$) and Zumaia ($\delta^{18}O$) sections. The $\delta^{13}C$ and $\delta^{18}O$ measurements from El Kef were performed on homogenized bulk powdered sediment on 39 samples. The El Kef samples were analyzed at the Leibniz Laboratory for Radiometric Dating and Stable Isotope Research of the Kiel University (Germany), using a Kiel IV carbonate preparation device connected to a MAT 253 mass spectrometer from ThermoScientific. The bulk $\delta^{18}O$ measurements from Zumaia were performed on 108 samples. The Zumaia samples were analyzed in the Department of Earth Sciences of the University of Oxford (United Kingdom), using a GasBench device attached to a ThermoFisher Delta V Advantage gas source isotope ratio mass spectrometer. All values for both sections are reported in the Vienna Pee Dee Belemnite notation (VPDB) compared to NBS-19 and IAEA-603 standards (El Kef) and NBS-19 and NBS-18 standards (Zumaia). Repeated analyses of in-house standards suggest a reproducibility ($\pm 1\sigma$) with a standard error of the laboratory internal and international standards (NBS-19, NBS-18 and IAEA-603) of <0.05‰ for $\delta^{13}C$ and of <0.09‰ for $\delta^{18}O$ values. The new isotope datasets are compared with those previously reported at ODP-1262 (Kroon and Zachos, 2007; Woelders et al., 2017), ODP-1049 (Quillévéré et al., 2008), ODP-1209 (Hull et al., 2020), Gubbio (Coccioni et al., 2010, 2012; Sinnesael et al., 2016), Caravaca (Gilabert et al., 2021a, 2021b), and Zumaia (Gilabert et al., 2022). The complete isotopic dataset is summarized in Table S1 (Appendix A).

2.2. Planktic foraminifera (triserial guembelitriids and aberrant specimens)

We evaluated environmental changes using two planktic foraminiferal proxies of environmental stress: relative abundance of triserial guembelitriids (*Guembelitria* and *Chiloguembelitria*), and relative abundance of aberrant specimens, or foraminiferal abnormality index (FAI), both measured in the >63 μm sieved fraction. For the guembelitriids abundance, we rely on the previously published quantitative dataset from Caravaca (Gilabert et al., 2021a, 2021b), Zumaia (Gilabert et al., 2022), Gubbio (Coccioni et al., 2010), El Kef and Aïn Settara (Arenillas et al., 2018), ODP-1262 (Krahl et al., 2023), DSDP Site 525 (Abramovich and Keller, 2003), and ODP-1209 (Hull et al., 2011). For the FAI, we used the quantitative studies from El Kef and Aïn Settara (Arenillas et al., 2018), DSDP Site 577 (Gerstel et al., 1986) and ODP-1262 (Krahl et al., 2023), and new quantitative data from the Spanish sections. For

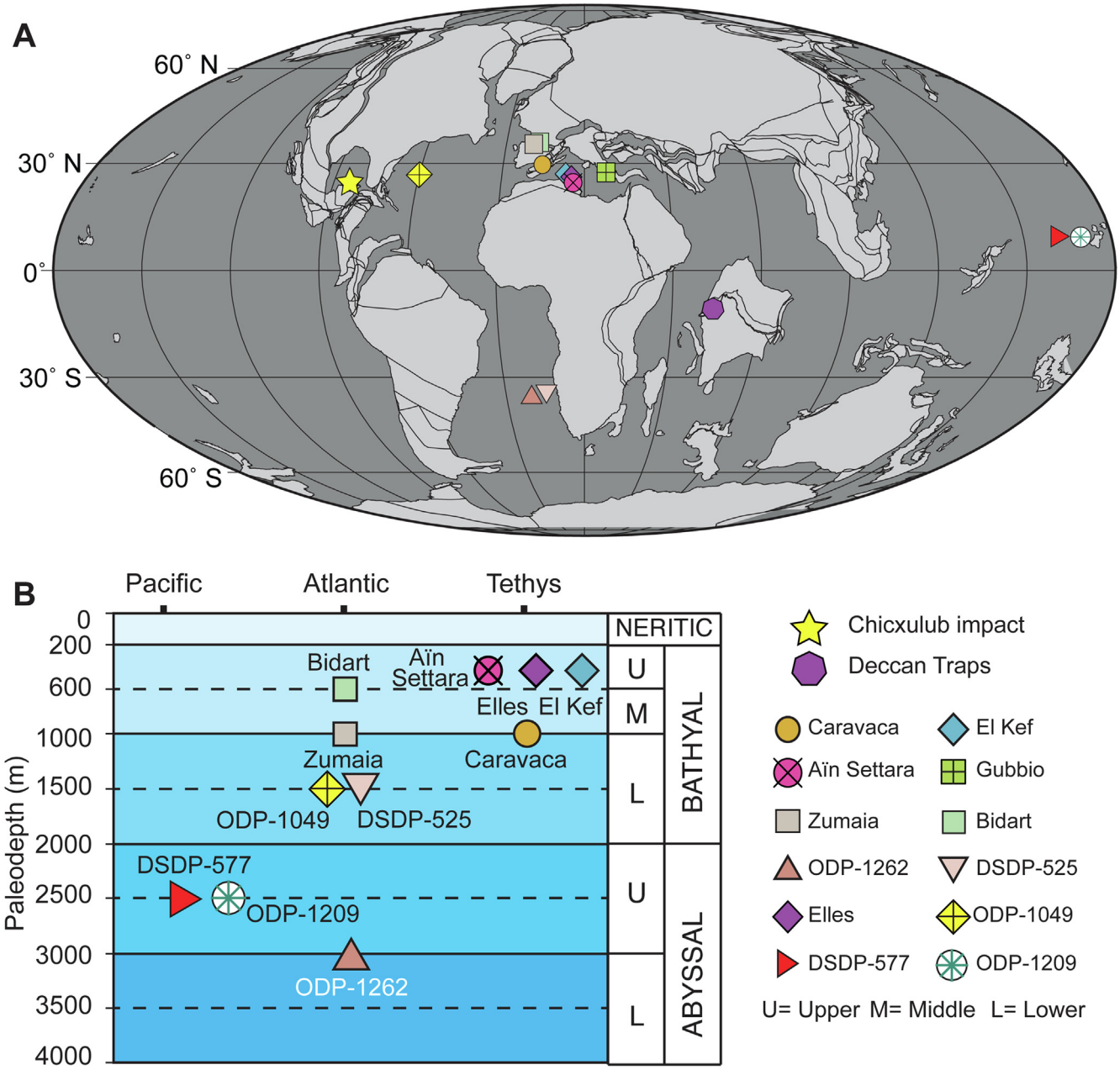

Fig. 1. A. Paleogeographic reconstruction for the Cretaceous-Paleogene boundary (~66 Ma; after https://www.odsn.de/odsn/services/paleomap/adv_map.html). **B.** Paleobathymetric reconstruction for the KPB (66 Ma), including the localities cited in this study. Estimated paleodepths are based on: Arenillas et al. (2018) for El Kef and Aïn Settara, Gilabert et al. (2021a, 2022) for Caravaca and Zumaia, Keller et al. (2020) for Elles, Font et al. (2022) for Bidart, Li and Keller (1998) for DSDP Site 525, Gerstel et al. (1986) for DSDP Site 577, Barnet et al. (2019) for ODP Site 1262, and Westerhold et al. (2011) for ODP Site 1209. (For interpretation of the references to colour in this figure legend, the reader is referred to the web version of this article.)

the latter, we studied 67 samples from Zumaia, and 14 new samples from the Maastrichtian of Caravaca, which complements the Danian quantitative study by Gilabert et al. (2021b) for the same locality. The complete foraminiferal dataset is summarized in Table S2 (Appendix A). For recognition of aberrant morphologies, we follow the guidelines of Arenillas et al. (2018). Our new results are compared with other quantitative analyses of aberrant planktic foraminifera from Caravaca (Gilabert et al., 2021b), El Kef and Aïn Settara (Arenillas et al., 2018), ODP-1262 (Krahl et al., 2023), and DSDP Site 577 (Gerstel et al., 1986). Examples of aberrant specimens from different localities are illustrated in Fig. 2.

2.3. Mercury enrichments

Volcanoes are considered a primary source of Hg to the atmosphere (Grasby et al., 2019) and it has been proposed that Hg enrichments in some late Maastrichtian–early Danian sedimentary sections are the result of Deccan Traps volcanic activity. For this reason, we have compiled some of the most recently published Hg concentrations across the KPB, from ODP-1049 (Nauter-Alves et al., 2023), ODP-1262 (Krahl et al., 2023), Zumaia (Font et al., 2018; Percival et al., 2018), Bidart (Font et al., 2022), and Elles (Keller et al., 2020). Mercury is commonly presented normalized

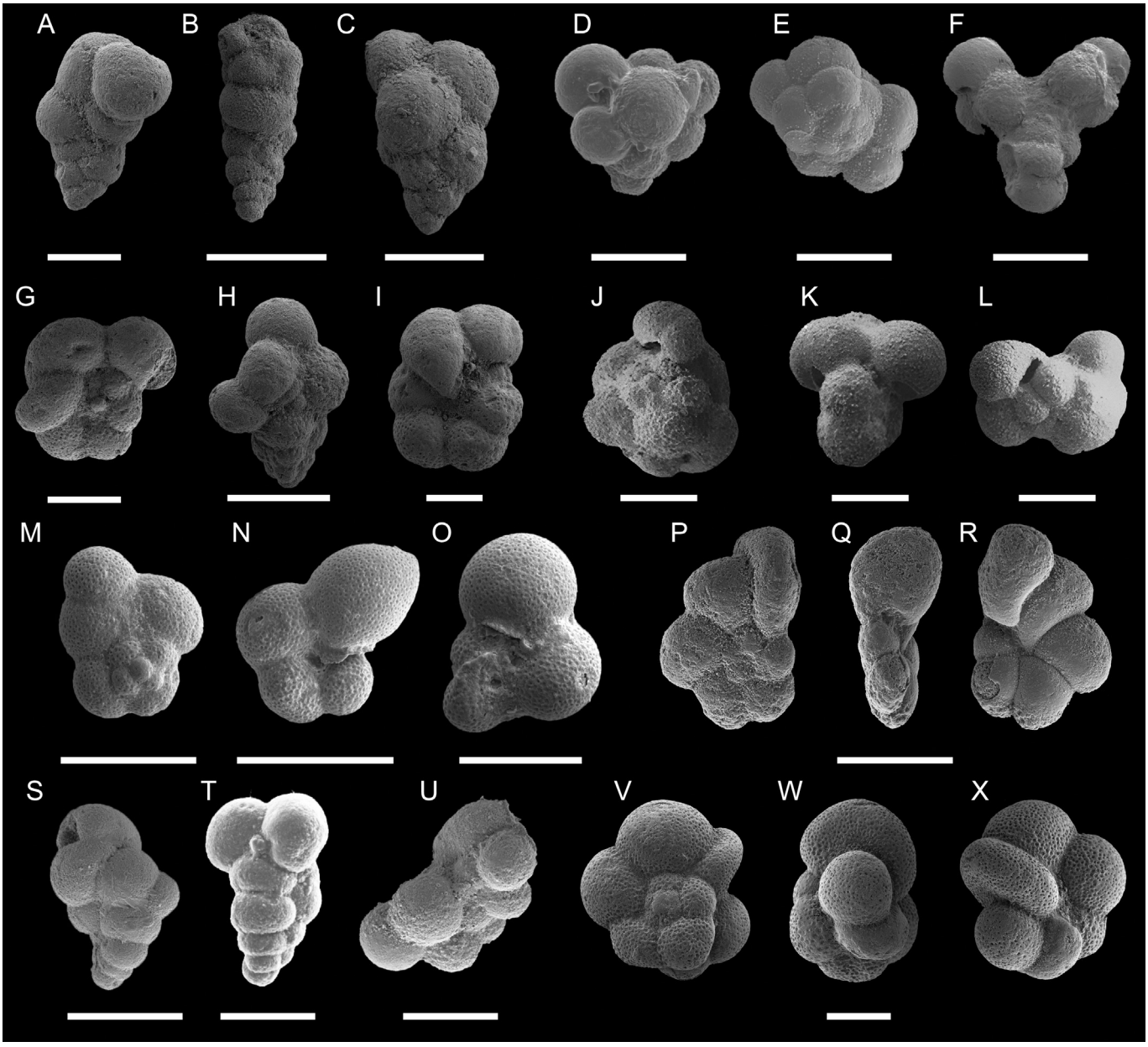

Fig. 2. Examples of extreme aberrant specimens of early Danian planktic foraminifera. **A-C.** Specimens from Zumaia (this study). A: aberrant shape of last chamber; B: anomalous position of last chamber (uniserial); C: kummerform or reduced last chamber. **D, E**. Specimens from El Kef (Arenillas et al., 2018). D: proliferation of chambers (multiserial); E: abnormally spiroconvex test. **F.** Attached triplets (triamese). **G-I.** Specimens from Caravaca (Gilabert et al., 2021b). G: aberrant chamber; H: additional chamber; I: aberrant chamber. **J-L.** Specimens from DSDP-577 (Gerstel et al., 1986). J: monstrous test; K: double twined chambers; L: attached twins (siamese). **M-O.** Specimens from ODP Site 1262 (Krahl et al., 2023). M: additional chamber; N: aberrant shape of last chamber; O: aberrant chamber. **P-R.** Specimens from El Kef (Arenillas et al., 2018). Abnormally compressed test and aberrant ultimate chamber. **S-U.** Specimens from Aïn Settara (Arenillas et al., 2018). S: kinking (two rotation axes); T: double twined chambers; U: monstrous test. **V-X.** Specimens from El Kef (Arenillas et al., 2018). Lack of sculpture in the test, with bulla-like antepenultimate chamber and two kummerform last chambers. Scale bars: 100 μm.

to total organic carbon (TOC), to account for its strong affinity to organic matter. Therefore, the Hg/TOC ratio is preferably used to evaluate the volcanic contribution to the Hg anomalies (Grasby et al., 2019), although comparison with Al_2O_3 can be used when TOC values are <0.1% (Percival et al., 2018). The compiled Hg records are shown in Table S3 (Appendix A).

3. Results

3.1. Age models

Age models are based on three types of data: (*i*) cyclostratigraphic data, (*ii*) planktic foraminiferal biostratigraphic data, and (*iii*) magnetostratigraphic data. As core age model, we used the astronomical age models, based on the 405-kyr eccentricity cycle tuning, of Dinarès-Turell et al. (2014) for the early Danian and of for the Maastrichtian. Both Danian and Maastrichtian models were developed at Zumaia, and have recently been combined and updated by Gilabert et al. (2022). For ODP Sites 1209 and 1262, the early Danian 405-kyr eccentricity tuning of Dinarès-Turell et al. (2014) was applied. For the Maastrichtian of Sites 1209 and 1262, we used the age models proposed by Westerhold et al. (2011) and Woelders et al. (2017), respectively. The tie-points for age calibration were the 405-kyr maxima and minima extracted from the La2011 astronomical solution (Laskar et al., 2011). For consistency, we assign a KPB age of 66.001 Ma as proposed by

Dinarès-Turell et al. (2014) and the Geological Time Scale 2020 (Gradstein et al., 2020). This age for the KPB differs from latest U-Pb and $^{40}Ar/^{39}Ar$ dating with ages of 66.016 ± 0.05 Ma (Schoene et al., 2019) and 66.052 ± 0.008/0.043 Ma (Sprain et al., 2018), respectively, but it falls within the uncertainties of the systematic error of both techniques. For localities with unavailable cyclostratigraphic data, we used the biochronological age model of Gilabert et al. (2022) with planktic foraminifera (for details, see Suppl. Text and Fig. S1, Appendix A). For the magnetochronological age model, we use the ages given by Gradstein et al. (2020) for the C30n/C29r magnetic reversal (66.31 Ma) and those reported by Dinarès-Turell et al. (2014) for the C29r/C29n and C29n/C28r magnetic reversals (65.700 and 64.958 Ma, respectively). Furthermore, at El Kef, Gubbio and Caravaca, we establish chemostratigraphic correlations with the astronomically tuned Zumaia section, allowing to refine their age models. Finally, an age interpolation for every sample was performed assuming a constant sedimentation rate between the anchored tie-points (i.e., 405 kyr maxima and minima, magnetic reversals and bioevents). Details for the different age models are shown in Fig. S2 and Table S4 (Appendix A).

3.2. New isotopic dataset

The new bulk isotopic record at the El Kef section shows a low degree of correlation between $\delta^{13}C$ and $\delta^{18}O$ (r = 0.304, p < 0.01, n = 39), suggesting that primary isotopic trends are preserved (Swart, 2015). The $\delta^{13}C$ values range between −1.49‰ and 1.72‰ with an average value of 0.16‰ for the entire section, and between 0.92‰ and −0.31‰ for the Maastrichtian and the Danian, respectively. The $\delta^{18}O$ values varies between −3.79‰ and −2.68‰ with an average value of −3.21‰ for the entire section, and 0.92‰ and −0.31‰ for the Maastrichtian and the Danian, respectively. Isotopic values obtained here are consistent with previous isotopic analyses carried out at El Kef (Keller and Lindinger, 1989; Jones et al., 2023). The $\delta^{18}O$ values obtained for the Zumaia section correspond to the $\delta^{13}C$ values of the same sample-set already published in Gilabert et al. (2022). Although correlation between $\delta^{13}C$ and $\delta^{18}O$ values seems quite high (r = 0.73, p < 0.01, n = 108), this seems to be due to parallel trends in $\delta^{13}C$ and $\delta^{18}O$ values across the section. For both O and C, the same isotopic trends are maintained across the Upper Maastrichtian-lowermost Danian interval, i.e., 4.55 m below to 0.25 m above the KPB. Similar trends are recognized in other open marine sections, such as Caravaca, El Kef or Gubbio (Fig. S2; Appendix A), suggesting that the primary isotopic trends at Zumaia are preserved. The remaining early Danian samples (i.e., ∼0.25 cm to 8.5 m above the KPB) show low correlation between $\delta^{13}C$ and $\delta^{18}O$ values (r = 0.33, p < 0.01, n = 59), suggesting that, although diagenesis could exert some control in the $\delta^{18}O$ record across the lower portion of the Zumaia section, overall isotopic trends are preserved. The detailed evolution of the isotopic records of both El Kef and Zumaia is dissected and compared with the other studied localities (Caravaca, Gubbio, ODP-1262 and ODP-1209) below, in the discussion section.

4. Discussion

4.1. Last 100 kyr of the Maastrichtian

According to the stable isotope dataset compiled here, the latest 100 kyr of the Maastrichtian show a robust trend towards increasing (more positive) bulk $\delta^{18}O$ and $\delta^{13}C$ values of ca. 1.2‰ and 1.3‰, respectively, for Caravaca; 0.8‰ and 0.9‰ for Zumaia; 0.6‰ and 1.4‰ for El Kef; 1.0‰ and 0.2‰ for Gubbio; 0.3‰ and 0.6‰ for ODP-1262; and 0.3‰ and 0.2‰ for ODP-1209 (Fig. 3). These values reflect a return to the general global cooling trend of the Maastrichtian after the peak of the Late Maastrichtian Warming Event approximately ∼150 kyr before the KPB (Li and Keller, 1998; Hull et al., 2020). This cooling of the sea surface is mimicked by a similar cooling trend in the deep sea observed in benthic foraminiferal records (Westerhold et al., 2011; Barnet et al., 2018). This gradual and stable latest Cretaceous climatic cooling questions the hypothetical role of Deccan volcanism in the climate of the last tens of thousands of years of the Maastrichtian (Schoene et al, 2019).

The changes in the Hg/TOC ratio during this interval are very variable in each locality (Fig. 4). While distinct Hg enrichments are recorded at Bidart and Elles in the last ∼30–15 kyr of the Maastrichtian (Keller et al., 2020; Font et al., 2022); no significant changes are identified at Zumaia (Font et al., 2018), ODP-1262 (Krahl et al., 2023), Brazos River, USA (Percival et al., 2018), and Wasserfallgraben, Germany (Regelous et al., 2022) during this interval. Local scavenging and post-depositional processes penetrating the uppermost Maastrichtian (Smit, 2016) and greater terrigenous runoff (Percival et al., 2018) have been proposed as potential explanations for the occasional enrichment of Hg below the KPB. In general, the environmental effects expected as a result of volcanism, such as carbonate dissolution, have not been reported in the localities studied (Gilabert et al. 2021a; Barnet et al., 2018), although Font et al. (2018) identified akageneite within the last meters of the Maastrichtian from Zumaia, and interpreted it as evidence for continental magnetite dissolution by acid rains. In any case and according to Henehan et al. (2019), oceanic pH remained stable during the last ∼100 kyr of the Maastrichtian, negating a widespread ocean acidification episode in the latest Maastrichtian as suggested by Keller et al. (2020).

Mean relative abundances in opportunistic *Guembelitria* are low during the last 100 kyr of the Maastrichtian: 1.69% at Caravaca, 2.15% at Zumaia, 1.75% at El Kef, 2.92% at Aïn Settara, and 0% at DSDP Site 525 (Fig. 5; Table S2, Appendix A). No values for ODP-1209 nor for DSDP Site 577 have been considered since both cores are severely affected by contamination by planktic foraminiferal specimens from the overlying basal Paleocene (Jouini et al., 2023). Mean relative abundances in planktic foraminiferal aberrant specimens for the same interval are also low: 0.6% at Caravaca, 0.3% at Zumaia, 0.6% at El Kef, and 1.8% at Aïn Settara (Fig. 5; Table S2, Appendix A). Therefore, if the Poladpur volcanic pulse did take place at the end of the Maastrichtian rather than the earliest Danian, it seems to have had very little climatic and paleobiological impact on open ocean settings, as indicated by the low frequency of *Guembelitria* specimens (generally <3%) and of aberrant specimens (generally <2%), suggesting environmental conditions remained stable during this interval.

4.2. Paleoclimatic and paleoenvironmental trends during the first ∼10 kyr of the Danian: The KPB and the dark clay bed

The KPB displays a very sharp negative carbon isotope excursion (CIE) in all the analyzed localities (Fig. 3(A), 6(A)). The $\delta^{13}C$ values remain low across the well-known KPB dark clay bed deposited, according to Gilabert et al. (2021b), during the first ∼10 kyr of the Danian. The KPB dark clay bed CIE, albeit very well developed in all the sections, is more pronounced in the shallower Tethyan sections, with drops in $\delta^{13}C$ of ca. −2.7‰, −2.3‰, −2.0‰, and −1.0‰ for El Kef, Caravaca, Zumaia, and Gubbio, respectively. For ODP Sites 1262 and 1209, the decrease in $\delta^{13}C$ is ca. −0.6‰, while for ODP-1049 it is −0.9‰ (Fig. 3(A); Table S1, Appendix A). It has been proposed that higher remineralization of refractory material in the surface ocean, together with inefficient export to the deep-sea due to collapse of marine ecosystems could explain the extremely low $\delta^{13}C$ values at the KPB event (Henehan et al., 2019; Bralower et al., 2020). The bulk $\delta^{18}O$ record displays a similar pat-

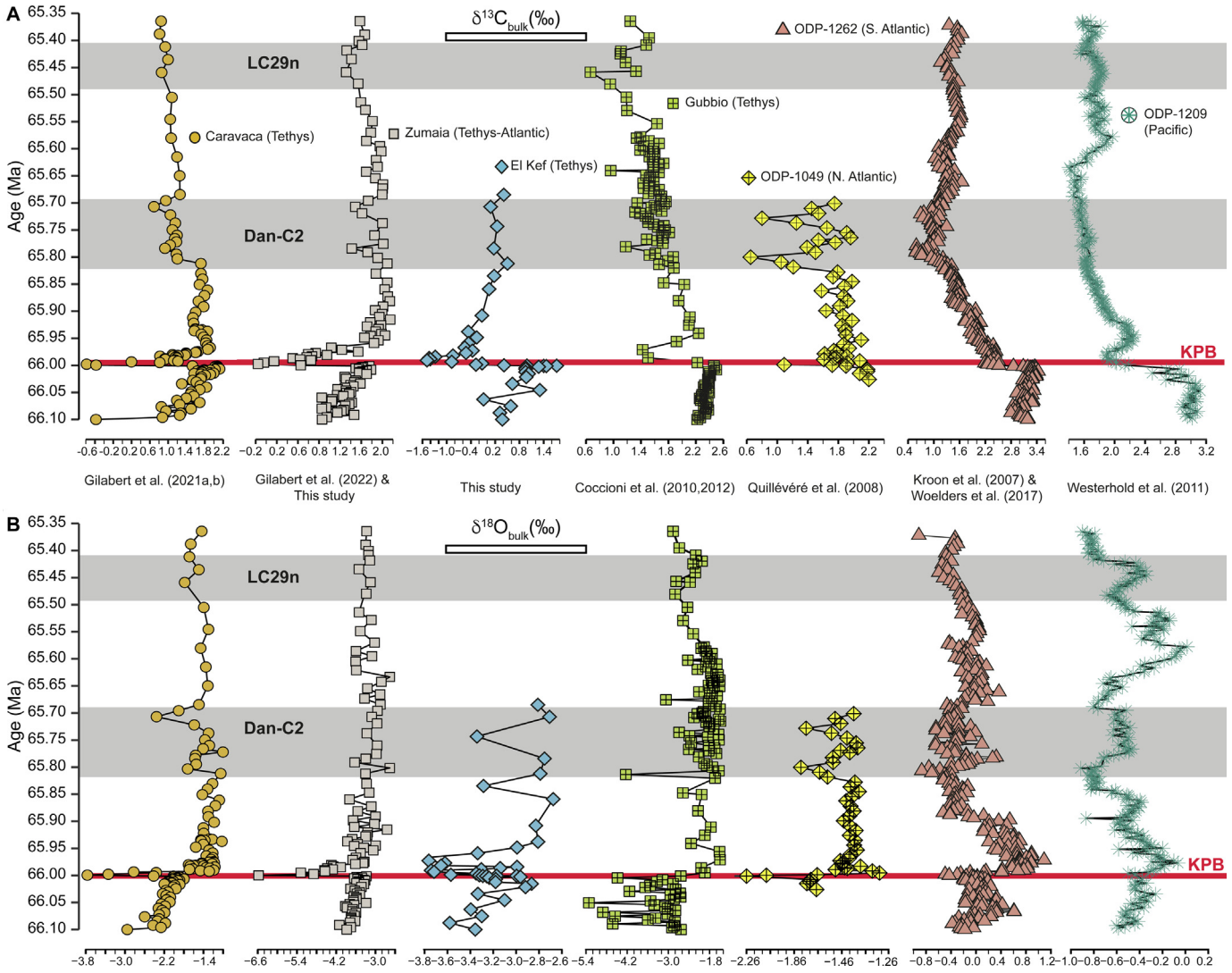

Fig. 3. Temporal correlation of bulk $\delta^{13}O$ (**A**) and bulk $\delta^{18}O$ (**B**) records across the Cretaceous-Paleogene transition (66.10 to 66.35 Ma). Gray shading marks the Dan-C2 and LC29n events. (For interpretation of the references to colour in this figure legend, the reader is referred to the web version of this article.)

tern as $\delta^{13}C$, with a sharp negative oxygen isotope excursion (OIE) at the KPB briefly disrupting the latest Maastrichtian cooling trend. The KPB OIE is recognized in all the studied localities, except for ODP-1209.

Several severe environmental and climatic consequences of the Chicxulub impact are proposed to have taken place immediately after the KPB, including global warming, changes in oceanic productivity, surface ocean acidification, heavy metal pollution, and eutrophication (Birch et al., 2016; Henehan et al., 2019; Hull et al., 2020). The contribution of Deccan volcanism to these climatic/environmental effects are still poorly constrained (Hull et al., 2020), although they should not be entirely discarded. The greatest Hg/TOC anomaly of all studied localities is recognized at the KPB of Elles (~6000), but Bidart also shows a considerable enrichment (Keller et al., 2020; Font et al., 2022). This short-lived early Danian Hg anomaly (Figs. 4, 6(B)) has been linked to the Chicxulub impact (Smit et al., 2016), but Deccan volcanism could also have contributed to the Hg anomalies identified immediately above the KPB. In addition, it is unclear whether the release of toxic heavy metals other than Hg (e.g., nickel, thallium, lead or tellurium), typically attributed to the Chicxulub impact, can also be explained by the onset of intense Deccan volcanism at the KPB (Regelous et al., 2022). Some heavy metals could have long oceanic residence times (Jiang et al., 2010), which in combination with the weathering of contaminated surface sediments, could have contributed to prolong their deposition for thousands of years after the KPB (Arenillas et al., 2018). Therefore, the enrichment of toxic metals derived from both the Chicxulub impact and Deccan eruptions could explain the trace element composition and paleobiological response recorded in the KPB dark clay bed (Gilabert et al., 2021b).

Immediately after the KPB catastrophic mass extinction, a sharp bloom of opportunistic *Guembelitria* is identified in open ocean localities (Arenillas et al., 2018, 2022; Gilabert et al., 2022; Figs. 5, 6(B)). A similar bloom is recognized in the opportunistic-eutrophic calcareous dinoflagellate *Thoracosphaera*/*Cervisella* (Jones et al., 2019). The *Guembelitria* bloom is better recorded in localities where the KPB dark clay bed is more expanded, as at Caravaca and Zumaia (with a ~10 cm-thick dark clay bed; Gilabert et al., 2021b, 2022) and at El Kef and Aïn Settara (with a ~100 cm- and 65 cm-thick dark clay bed, respectively; Arenillas et al., 2018). At these four sections, average relative abundances of *Guembelitria* range between 80% to almost 100%, after considering the rest of the Cretaceous specimens as reworked (Arenillas et al., 2022). In addition to the *Guembelitria* bloom, the KPB dark clay bed is also characterized by a remarkable increase in planktic foraminiferal

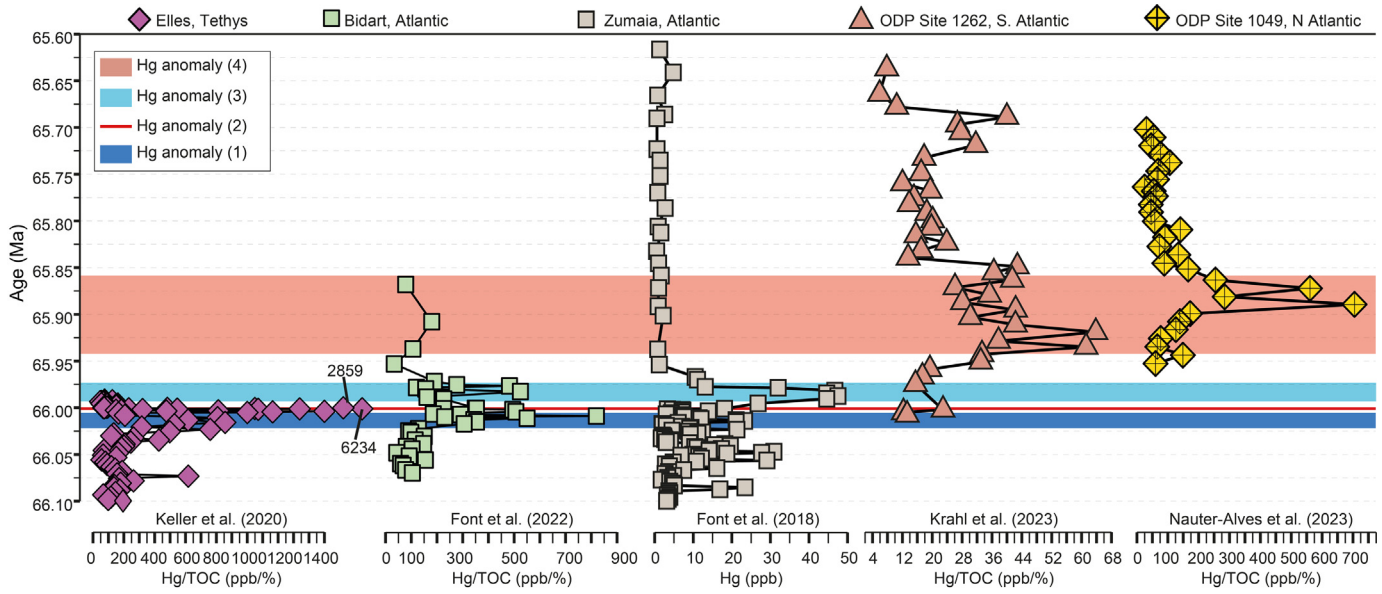

Fig. 4. Temporal correlation of the Hg datasets studied here. Late Maastrichtian to Early Danian Hg anomalies (1–3) fall within the uncertainty range of the radiometric ages of the Poladpur Fm. of the Deccan Traps. The Hg anomaly (2), corresponding to the KPB dark clay bed, could also be directly related to the Chicxulub impact. The Hg anomaly (4) is similar in age to the Ambenali Fm. of the Deccan Traps. (For interpretation of the references to colour in this figure legend, the reader is referred to the web version of this article.)

aberrant specimens, with FAIs between 15% and 20% at El Kef, Aïn Settara, Zumaia, Caravaca and DSDP-577 (Figs. 5, 6(B)). Increased FAIs usually coincide with high pollution levels (Arenillas et al., 2018), which are to be expected after the Chicxulub impact and a volcanic outburst in the Deccan, as we suggest here. It is noteworthy that the proliferation of aberrant specimens across this short stratigraphic interval is exclusively restricted to the genus *Guembelitria* and to the new incoming Danian taxa, mostly represented by tiny trochospiral genera *Parvularugoglobigerina* and *Palaeoglobigerina*, reinforcing the hypothesis that *Guembelitria* was the only planktic foraminifera survivor of the KPB (Arenillas et al., 2018, 2022; Gilabert et al., 2022).

4.3. From ~10 to 50 kyr after the KPB: Short and transient recovery

After the first 10 kyr of the Danian, which are characterized by the CIE-OIE of the KPB dark clay bed, most localities exhibit a trend towards more positive values in both $\delta^{13}C$ and $\delta^{18}O$ (Figs. 3, 6(A)), returning to values near those recorded before the KPB. Nonetheless, there are differences depending on locality: at Caravaca, Zumaia, Gubbio and ODP-1049, $\delta^{13}C$ reaches values similar to those of the uppermost Maastrichtian; at El Kef and the ODP-1209, the $\delta^{13}C$ recovery stops half way; and, at ODP-1262, the $\delta^{13}C$ increase is very small (Fig. 3(A), Fig. 6(A)). To identify the cause of these shifts, it must be considered that bulk $\delta^{13}C$ values are a mixture of isotopic signatures of multiple carbonate sources and diagenetic processes (Sepúlveda et al., 2019). Henehan et al. (2019) proposed that the initial surface ocean acidification after the KPB, together with the extinction of calcifying organisms, would have led to a transient reduction in the marine alkalinity sink. With the return of marine calcifiers, the excess of alkalinity in seawater was removed leading to a rapid rebound and overshoot in surface ocean pH ~50 kyr after the KPB (Henehan et al., 2019), which could condition the bulk $\delta^{13}C$ signal during the early Danian. Nonetheless, the bulk $\delta^{13}C$ record between ~66.0 and 65.95 Ma shows that the carbon cycle of the earliest Danian was characterized by a global positive shift. The $\delta^{18}O$ record also shows a positive shift, suggesting that sea-surface temperatures continued the trend towards cooling started in the latest Maastrichtian, which in fact coincided with a 405-kyr eccentricity minima according to the astronomical solution used here (Fig. 6). The Hg/TOC anomaly found at Bidart (Fig. 4; Hg anomaly 3) occurred above the iridium anomaly (Font et al., 2022), suggesting a rapid increase in the Deccan volcanic activity after the KPB. A similar Hg anomaly is recognized at Zumaia (Fig. 4) and it has also been reported at Wasserfallgraben (Regelous et al., 2022). According to our age model, this anomaly lasted for only ~18 kyr after the Chicxulub impact (Fig. 4; Table S4, Appendix A).

Between 10 and 50 kyr after the KPB, the relative abundance of *Guembelitria* decreased rapidly (Arenillas et al., 2018; Lowery et al., 2021; Gilabert et al., 2021b), suggesting less harmful conditions for calcareous plankton than those immediately after the KPB. This datum questions the significance of the above-mentioned volcanic event. Moreover, during this time, a bloom of parvularugoglobigerinids (*Parvularugoglobigerina* and *Palaeoglobigerina*) occurred, as well as the beginning of the second planktic foraminiferal evolutionary radiation, with the appearance of the slightly larger and more complex genera *Eoglobigerina*, *Globanomalina*, *Trochoguembelitria*, *Parasubbotina*, and *Praemurica*. Nevertheless, these incoming Danian genera still were scarce during this interval (Gilabert et al., 2022). Finally, the parvularugoglobigerinid bloom was replaced by a proliferation of the biserial genera *Woodringina* and *Chiloguembelina* about 30 or 40 kyr after the KPB (Arenillas et al., 2021; Gilabert et al., 2022).

In this interval, the average FAI is 10% at Caravaca, 13% at Zumaia, 8% at El Kef, 6.7% at Aïn Settara, and 4.5% at DSDP Site 577 (Figs. 5, 6(B); Table S2, Appendix A). These FAI values, although high, are lower than those of the first ~10 kyr after the KPB, reinforcing that maximum environmental stress was reached during the deposition of the KPB dark clay bed. It is noteworthy that the FAI at ODP-1262 is extremely low (~0.5%), which contrasts with the proliferation of aberrant specimens at localities relatively close to the continent, as in those from Tethys and DSDP Site 577 from the Pacific (Fig. 5). The FAI dataset suggests that the environmental perturbation at ODP-1262 (South Atlantic) was less intense during this interval in comparison to the localities evaluated in the Northern hemisphere, as also proposed by Jiang et al. (2010). An alternative explanation is that, after the devastation of calcareous

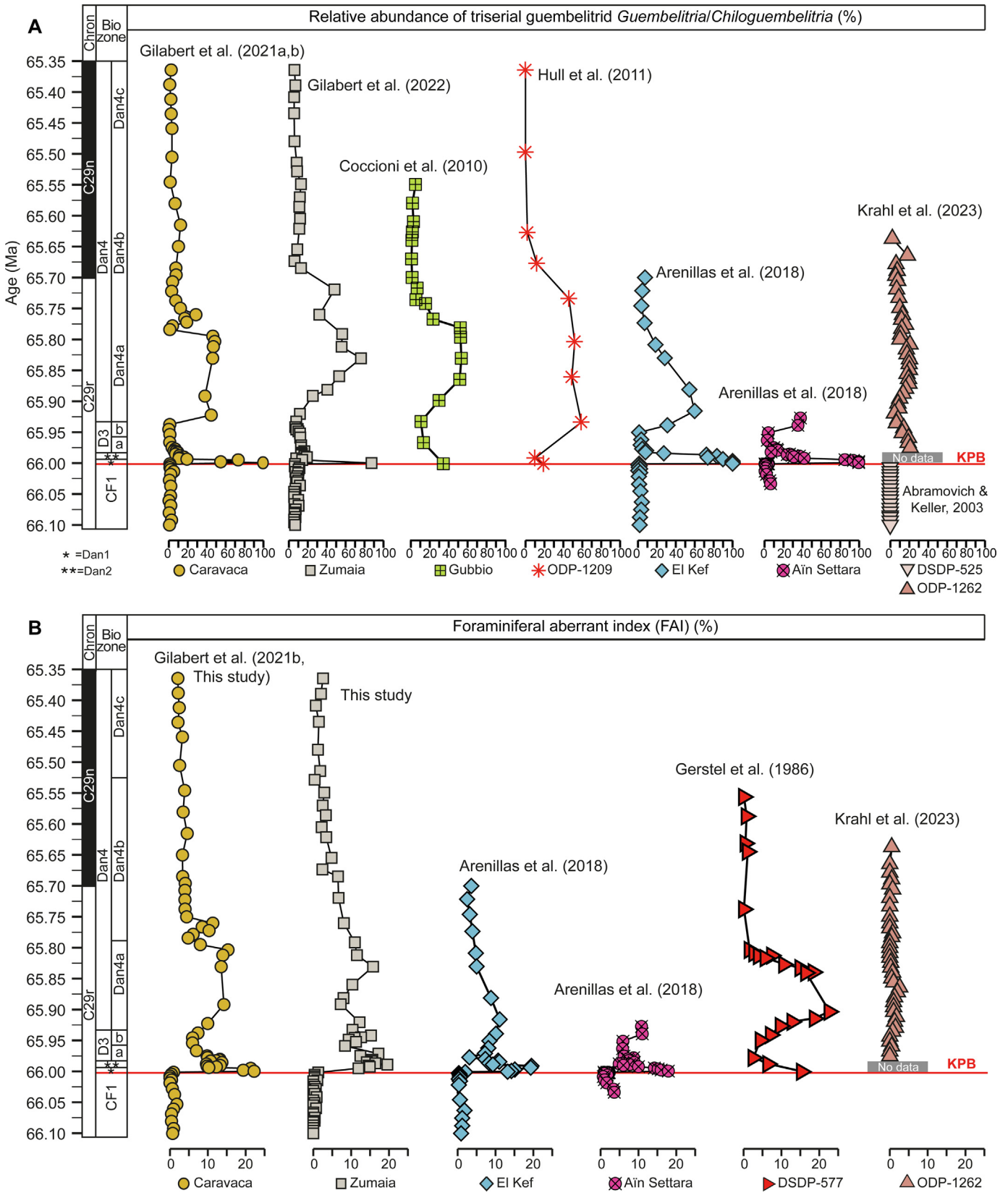

Fig. 5. Temporal correlation of the blooms of triserial guembelitriids and aberrant planktic foraminiferal specimens. **A.** Relative abundance of genera *Guembelitria* and *Chiloguembelitria* in the >63 µm sieved fraction. **B.** Foraminiferal abnormality index (FAI in %). The biozonation used here follows Arenillas et al. (2021) for the early Danian and Li and Keller (1998) for the Late Maastrichtian (see Appendix A: Supplementary Text for details). (For interpretation of the references to colour in this figure legend, the reader is referred to the web version of this article.)

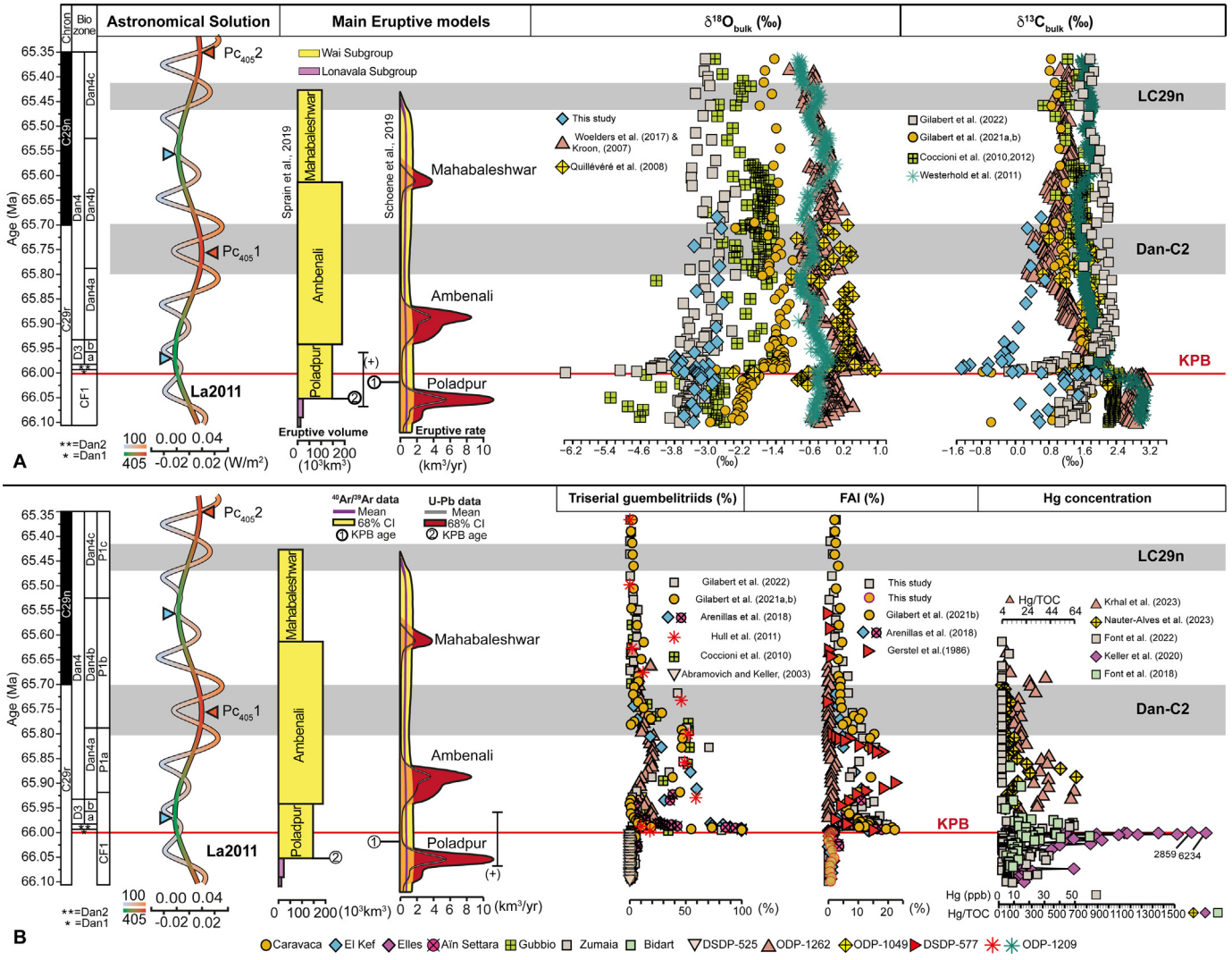

Fig. 6. Synthesis of the evolution of all environmental and climatic proxies investigated at the studied open-ocean localities, and position of all events recognized across the KPB. **A.** Bulk $\delta^{18}O$ and $\delta^{13}C$, whose excursions mark the KPB, Dan-C2 and LC29n events. **B.** Relative abundance in triserial guembelitriids (*Guembelitria* and *Chiloguembelitria*) and in the planktic foraminiferal aberrant specimens (FAI in %), whose blooms mark environmental stress episodes, and Hg concentrations, whose anomalies potentially mark volcanic episodes. All the used proxies are temporally correlated with: planktic foraminiferal zones of Arenillas et al. (2021) for the lower Danian, and Li and Keller (1998) for the uppermost Maastrichtian; the La2011 astronomical solution (Laskar et al., 2011); the Deccan eruptive models of Sprain et al. (2019) and Schoene et al. (2019); and the position of the C29r/C29n magnetic reversal based on Dinarès-Turell et al. (2014). Red and blue triangles: tie points of 405 kyr eccentricity maxima and minima, respectively; $Pc_{405}1$ and $Pc_{405}2$: 405 kyr eccentricity maxima 1 and 2 of the Paleocene; (+): uncertainty range for the KPB dating within the Deccan Traps; CI: confidence interval. (For interpretation of the references to colour in this figure legend, the reader is referred to the web version of this article.)

plankton at the KPB, the biological pump was globally weakened (Birch et al., 2016), but there was some degree of regional heterogeneity in the export productivity (Hull et al., 2011; Henehan et al., 2019), which could be locally higher by removing the excess of nutrients from the sea-surface more efficiently (Lowery et al., 2021).

4.4. From 50 to 300 kyr after the KPB: A second bloom of opportunistic triserial guembelitriids, and the Dan-C2 event

From ~65.95 to 65.80 Ma, $\delta^{13}C$ follows a gradual negative trend, where ODP Sites 1209 and 1262 display the greatest negative shift with drops of −0.6‰ and −1‰, respectively (Fig. 3(A), Fig. 6(A)). ODP-1049 shows a moderate drop of ca. −0.2‰, while Caravaca and Zumaia seem to fluctuate around a stable average, similar to values recorded for the uppermost Maastrichtian. El Kef is the only locality with an increase, of ca. 0.8‰. Similarly, bulk $\delta^{18}O$ shows the greatest decrease at ODP Sites 1209 and 1262, of −0.8‰ and −1.2‰, respectively. Nevertheless, at Caravaca, Zumaia, Gubbio, El Kef and ODP-1049, bulk $\delta^{18}O$ values display almost no change, although some few negative peaks can be recognized (Fig. 3(B), Fig. 6(A)). Simultaneously, in the interval ~65.95–65.8 Ma (i.e., 50–200 kyr after the KPB), a remarkable second bloom of the opportunistic triserial guembelitriids, specifically of *Chiloguembelitria*, a Danian descendant of *Guembelitria* (Arenillas et al., 2018), has been identified in all the studied sections, reaching maximum values that range between 40% and 60% in most localities (Fig. 5 (A)). Only ODP-1262 shows values <40%, but reaches around 20–25% during the same time interval. The contemporaneity of *Chiloguembelitria* blooms in all the studied localities suggests that the perturbation that drove this biological response was indeed global. The isotopic record does not show clear changes during this interval, and therefore increases in opportunistic taxa do not seem to be linked to a sudden change in sea-surface temperatures as other authors have proposed (Abramovich and Keller, 2003; Keller et al., 2020). *Guembelitria*/*Chiloguembelitria* often inhabit

nutrient-rich, shallow waters near continental margins and volcanic areas (Arenillas et al., 2018). Therefore, an intensive and global environmental disturbance at the sea-surface is required to explain this new proliferation of triserial guembelitriids in open marine localities. A possible explanation is that the emplacement of the largest volume Wai formations of the Deccan flood basalts may have increased heavy metals and nutrients in the the sea-surface, contributing to the bloom of triserial taxa and the rise in FAI observed during this period in all studied localities (Gilabert et al., 2022; Figs. 5, 6(B)). The Hg/TOC records of Bidart, ODP-1262 and ODP-1049 show a remarkable Hg anomaly between ~65.95 and 65.85, with the higher values recorded in North Atlantic ODP-1049 (Nauter-Alves et al., 2023; Font et al., 2022; Krahl et al., 2023). It is noteworthy that this Hg anomaly cannot be recognized at Zumaia (Figs. 4, 6(B)). This could be explained by the higher sedimentation rate recognized at Zumaia for this interval (1.52 cm/kyr) compared with the other localities for the same time interval: Bidart (1.05 cm/kyr), ODP-1049 (0.02 cm/kyr), and ODP-1262 (0.006 cm/kyr). Therefore, it is possible that, during this interval, the higher sedimentation rate at Zumaia could have led to dilution of the volcanic Hg signal and overprinting with detrital Hg, which would explain the very low Hg concentrations in this section. In any case, and excluding the Zumaia Hg record for this interval, the Hg anomaly between 65.95 and 65.85 Ma can be temporally correlated to the emplacement of the Ambenali Fm. of the Deccan Traps (Schoene et al., 2019; Sprain et al., 2019), suggesting a mechanistic relationship between volcanism and environmental perturbation during this interval. Explaining why the blooms of triserial guembelitriids and aberrant specimens lasted slightly longer than the Hg anomaly (Fig. 6(B)) requires further investigation. Nevertheless, the very weak and inefficient biological pump that characterizes this interval could have prolonged the residence time of nutrients on a time scale of 10^4–10^5 years (Jiang et al., 2010) and explain the different duration of the blooms with respect to the Hg anomaly. In addition, recycling of refractory material in the surface ocean during the earliest Danian (Henehan et al., 2019; Lowery et al., 2021) could have contributed.

The gradual decreasing $\delta^{13}C$ trend is interrupted by a double spiked CIE known as Dan-C2 event (Quillévéré et al., 2008). According to our compilation, this isotopic event occurred between ~65.8 and 65.7 Ma and can be recognized in all the Atlantic and Tethyan sections studied here (Fig. 3(A), Fig. 6(A)). Its absence in Pacific Site ODP-1209 (Fig. 3(A)), together with the lack of evidence for deep-sea warming and carbonate dissolution (Barnet et al., 2019), questions the hyperthermal nature of the Dan-C2 event as originally proposed (Quillévéré et al., 2008). However, whereas the bulk $\delta^{13}C$ signature of all the Atlantic and Tethyan localities shows the characteristic double spiked CIE, the $\delta^{18}O$ records do not display the same pattern as described by Quillévéré et al. (2008) with only Caravaca showing a concurrent double spiked OIE (Fig. 3(B)). This reinforces the non-hyperthermal nature of Dan-C2, since a clear warming trend is not common according to the available isotopic records (Hull et al., 2020; Bazeen et al., 2024). Another possibility is that the bulk $\delta^{18}O$ values are diagenetically overprinted (Sepúlveda et al., 2019).

Although we do not consider it to be an hyperthermal event, the Dan-C2, like most of the Paleogene hyperthermals, seems modulated by changes in the eccentricity of the Earth's orbit (Galeotti et al., 2015; Barnet et al., 2019). Both Barnet et al. (2019) and Gilabert et al. (2022) found that the Dan-C2 event correlates well with the first 405 kyr eccentricity maximum of the Danian ($Pc_{405}1$), and its two symmetric CIEs correlate with two 100 kyr eccentricity maxima within the $Pc_{405}1$ maximum (Fig. 6(A)). However, some authors have proposed that the Dan-C2 event could have been triggered by Deccan volcanism (Coccioni et al., 2010; Krahl et al., 2020), although recent estimates of volcanic CO_2 outgassing argue against Deccan volcanism as a trigger of the Dan-C2 event (Fendley et al., 2020; Hull et al., 2020). Moreover, Hg enrichments, which appear to be the most direct evidence of volcanic activity, first occurred ~100 kyr before the onset of the Dan-C2 event (Fig. 6(B)), suggesting the latter is not directly related to the Deccan volcanism.

On the other hand, the *Chiloguembelitria* bloom clearly precedes the Dan-C2 event onset (Fig. 6(B)), and the abundance of these triserial guembelitriids decreases during the Dan-C2 event, reaching their typical values in open marine environments of <5–10%. During this event, planktic foraminiferal taxa inhabiting the thermocline and sub-thermocline, such as *Chiloguembelina*, *Eoglobigerina*, *Parasubbotina*, and *Subbotina*, start to became more abundant, suggesting an increase in the water column stratification and a first step towards the recolonization of deeper marine environments (Gilabert et al., 2021b, Krahl et al., 2023; Farouk et al., 2023). However, it is well-known that the entire reoccupation of the deeper ocean niches and the return to pre-KBP planktic foraminiferal diversity took several million years (Birch et al., 2016).

4.5. From 300 to 650 kyr after the KPB: End of Deccan volcanism, redefining the LC29n event and stabilization in the surface ocean

After the Dan-C2 event, a return to the gradual decreasing trend in $\delta^{13}C$ is observed until the end of the studied interval (Fig. 3(A), Fig. 6(A)). The deepest localities, ODP Sites 1262 and 1209 (Fig. 1), show some differences in comparison with the shallower ones (Fig. 3(A)). ODP-1262 displays a change towards higher isotopic values from the end of Dan-C2 event at ~65.7 Ma until 65.55 Ma, briefly interrupted by a transient decrease in $\delta^{13}C$ values culminating around 65.62 Ma (Fig. 3(A)). On the other hand, ODP-1209 follows the decreasing isotopic trend for $\delta^{13}C$ after the time interval corresponding to the Dan-C2 event until ~65.63 Ma, after which it follows the same positive shift as ODP-1262 until ~65.57 Ma. From this time until the end of the investigated interval, both sites resume a subtle decreasing isotopic trend in $\delta^{13}C$ values. The $\delta^{18}O$ record of Caravaca, Zumaia and Gubbio share a slight and gradually decreasing trend similar to the one recognized in their $\delta^{13}C$ bulk signatures (Fig. 3(A), Fig. 6(A)). Again, the deeper ODP Sites 1262 and 1209 display larger short-term changes, although the overall trend is towards lower $\delta^{18}O$ values, confirming the warming trend during most of the early Danian. At ODP-1209, from the end of the interval corresponding to the Dan-C2 event (i.e., from 65.7 Ma to 65.57 Ma), $\delta^{18}O$ increases by 0.8‰, reaching the highest values of the entire studied interval (Fig. 3 (B), Fig. 6(A)). At 65.57 Ma, $\delta^{18}O$, like $\delta^{13}C$, changes to an overall decreasing trend, as recorded in the shallower sites, although with some fluctuation during this interval (Figs. 3, 6(A)).

Between the Dan-C2 event and the following hyperthermal or carbon cycle perturbation (the low C27r event) ~2.4 myr elapsed (Galeotti et al., 2015). The only climatic event described between these two is the LC29n event, which was originally defined by Coccioni et al. (2010) at Gubbio, where it is characterized by a single point negative $\delta^{13}C$ excursion of ~0.5‰. Here we propose that the CIE identified at Zumaia, ODP-1262, Gubbio and Caravaca between ~65.47 Ma and 65.42 Ma (530–580 kyr after the KPB; Fig. 3(A), Fig. 6(A)) is the LC29n event, and thus we consider that the LC29n event is younger than proposed by Coccioni et al. (2010). At these localities, $\delta^{13}C$ values consistently decreased between ~0.2‰ and 0.4‰ during the LC29n event. Moreover, a small OIE is recognized at ~65.45 Ma in all the localities, approximately in the middle part of the LC29n event (Fig. 3(B), Fig. 6(A)). However, as in the case of Dan-C2 event, no clear warming of the ocean floor has been reported at the LC29n event (Hull et al., 2020). The trigger of LC29n event seems unlikely to be related to the Deccan volcanism, since it occurred 200 kyr later than the

end of Deccan volcanism (Schoene et al., 2019) or, at most, at the end of the emplacement of Mahabaleshwar Fm. (Sprain et al., 2019; Fig. 6). Recent radiometric dating of the Boltysh impact, a 24 km-diameter crater in Ukraine, suggests an age of 65.39 ± 0.14/0.16 Ma (Pickersgill et al., 2021), which coincides within the error range of age estimated here for the LC29n event. Although the exact mechanism behind LC29n event remains uncertain, its good temporal alignment with a 100 kyr eccentricity maxima (Fig. 6(A)) indicates that orbital forcing is the most likely trigger (Gilabert et al., 2022).

Towards the end of the Dan-C2 event at ~65.7 Ma, planktic foraminiferal assemblages became more diverse, with species belonging to genera of the second evolutionary radiation (*Eoglobigerina*, *Parasubbotina*, *Subbotina*, *Praemurica*, and *Globanomalina*) becoming progressively more abundant, until they collectively reach between 40% and 50% (Arenillas et al., 2021). The increase in the relative abundance of these species, which are mostly thermocline dwellers, ~300 kyr after the Dan-C2, suggests a more global and stable reoccupation of thermocline depths, which allows us to confirm that the stratification of the oceanic water column increased during this time (Lowery et al., 2021; Gilabert et al., 2021b; Krahl et al., 2023). With the available data, no relevant changes have been identified among the planktic foraminiferal assemblages during this interval, suggesting no severe environmental effects related to the emplacement of the Mahabaleshwar Fm., which spans the C29r–C29n transition. Similarly, during the LC29n event, the planktic foraminiferal assemblages exhibit only small-scale fluctuations, suggesting that no significant change in paleoenvironmental or palaeoceanographic conditions can be recognized (Gilabert et al., 2021b, 2022). No episodes of carbonate dissolution have been reported within the LC29n event in the localities studied here (Westerhold et al., 2011; Arenillas et al., 2018; Barnet et al., 2019; Gilabert et al., 2021b, 2022), indicating that this event was only a small climate/carbon cycle disturbance.

5. Conclusions

Our high-resolution multiproxy analysis from Pacific, Atlantic and Tethyan localities provides new evidence on the complex interplay between Deccan volcanism, the Chicxulub impact and orbital forcing across the Cretaceous-Paleogene boundary (KPB). Mercury (Hg) enrichments suggest increased volcanic activity between 30 kyr and 15 kyr before the KPB, which is tentatively attributed to the emplacement of the Poladpur Fm. of the Deccan Traps. However, in open marine localities, this volcanic activity did neither alter the planktic foraminiferal assemblages nor disrupt the gradual cooling trend of the Late Maastrichtian.

In addition to the planktic foraminiferal mass extinction, the Chicxulub impact triggered sudden climatic and environmental changes on the sea-surface during the first 10 kyr of the Danian, recorded as sharp negative carbon and oxygen isotopic excursions and blooms of triserial guembelitriids and aberrant specimens of planktic foraminifera. The origin of the Hg anomalies at the KPB are unclear, and both Chicxulub impact and Deccan volcanism can be potential sources for the Hg enrichments. The Hg anomalies dated at ~15–20 kyr after the KPB could be evidence of an acceleration of the Deccan volcanism (onset of the large-volume Wai formations) perhaps induced by the Chicxulub impact. However, if this Hg enrichment is due to volcanism, it clearly had not effect on the planktic foraminiferal assemblages. The last Hg anomaly recognized, dated at ~65.94–65.86 Ma, may be linked to the emplacement of the Ambenali Fm. This Hg anomaly is associated with a new bloom of triserial guembelitriids and aberrant specimens, indicating a new interval of environmental stress. Finally, our age model allows us to infer that the Deccan volcanism was not the trigger of the Dan-C2 and LC29n events, but these climate perturbations were more likely the result of orbital forcing.

CRediT authorship contribution statement

Vicente Gilabert: Writing – review & editing, Writing – original draft, Visualization, Resources, Methodology, Investigation, Data curation, Conceptualization. **Sietske J. Batenburg:** Writing – review & editing, Writing – original draft, Supervision, Methodology, Investigation, Conceptualization. **José A. Arz:** Writing – review & editing, Visualization, Supervision, Resources, Methodology, Investigation, Funding acquisition. **Nils B. Baumann:** Writing – review & editing, Visualization, Methodology. **Marcel Regelous:** Writing – review & editing, Methodology, Funding acquisition. **Ignacio Arenillas:** Writing – review & editing, Supervision, Project administration, Methodology, Funding acquisition.

Declaration of competing interest

The authors declare that they have no known competing financial interests or personal relationships that could have appeared to influence the work reported in this paper.

Acknowledgments

We deeply thank S. Galeotti and S. Farouk, for their detailed and constructive reviews. This research is part of the grants PID2022-136233NB-I00, funded by MCIN/AEI/10.13039/501100011033 and by ERDF A way of making Europe, and DGA group E33_23R, funded by the Aragonese Government and by ERDF A way of making Europe. Vicente Gilabert acknowledges support from Ministerio de Universidades (MIU) and European Union (Margarita Salas post-doctoral grant) funded by European Union NextGeneration EU. Marcel Regelous acknowledges funding from the Deutsche Forschungsgemeinschaft grant RE 3020/20-1.

Data availability

Data will be made available on request.

Appendix A. Supplementary material

Supplementary information (including a supplementary text, Figs. S1, S2, and Tables S1–S4) associated with this article can be found, in the online version, at https://doi.org/10.1016/j.geobios.2024.08.011.

References

Abramovich, S., Keller, G., 2003. Planktonic foraminiferal response to the latest Maastrichtian abrupt warm event: a case study from South Atlantic DSDP Site 525A. Marine Micropaleontology 48, 225–249.

Arenillas, I., Arz, J.A., Gilabert, V., 2018. Blooms of aberrant planktic foraminifera across the K/Pg boundary in the Western Tethys: causes and evolutionary implications. Paleobiology 44, 460–489.

Arenillas, I., Arz, J.A., Metsana-Oussaid, F., Gilabert, V., Belhai, D., 2022. Hypothesis testing on the planktic foraminiferal survival model after the KPB extinction: evidence from Tunisia and Algeria. Fossil Record 25, 43–63.

Arenillas, I., Gilabert, V., Arz, J.A., 2021. New biochronological scales of planktic foraminifera for the early Danian based on high-resolution biostratigraphy. Geosciences 11, 479.

Barnet, J.S.K., Littler, K., Kroon, D., Leng, M.J., Westerhold, T., Röhl, U., Zachos, J.C., 2018. A new high-resolution chronology for the late Maastrichtian warming event: establishing robust temporal links with the onset of Deccan volcanism. Geology 46, 147–150.

Barnet, J.S.K., Littler, K., Westerhold, T., Kroon, D., Leng, M.J., Bailey, I., Röhl, U., Zachos, J.C., 2019. A high-fidelity benthic stable isotope record of late cretaceous-early eocene climate change and carbon-cycling. Paleoceanography and Paleoclimatology 34, 672–691.

Bazeen, Y.S., Farouk, S., Elamri, Z., Ahmad, F., Al-Kahtany, K., Zaky, A.S., El-Sheikh, I., 2024. Planktic foraminifer response and paleoceanographic changes across the Danian – Selandian interval in the southern Tethys (Elles section, Central Tunisia). Palaeogeography, Palaeoclimatology, Palaeoecology 648, 112259.

Birch, H.S., Coxall, H.K., Pearson, P.N., Kroon, D., Schmidt, D.N., 2016. Partial collapse of the marine carbon pump after the Cretaceous-Paleogene boundary. Geology 44, 287–290.

Bralower, T.J., Cosmidis, J., Heaney, P.J., Kump, L.R., Morgan, J.V., Harper, D.T., Lyons, S.L., Freeman, K.H., Grice, K., Wendler, J.E., Zachos, J.C., Artemieva, N., Chen, S.A., Gulick, S.P.S., House, C.H., Jones, H.L., Lowery, C.M., Nims, C., Schaefer, B., Thomas, E., Vajda, V., 2020. Origin of a global carbonate layer deposited in the aftermath of the Cretaceous-Paleogene boundary impact. Earth and Planetary Science Letters 548, 116476.

Coccioni, R., Frontalini, F., Bancalà, G., Fornaciari, E., Jovane, L., Sprovieri, M., 2010. The Dan-C2 hyperthermal event at Gubbio (Italy): global implications, environmental effects, and cause(s). Earth and Planetary Science Letters 297, 298–305.

Dinarès-Turell, J., Westerhold, T., Pujalte, V., Röhl, U., Kroon, D., 2014. Astronomical calibration of the Danian stage (Early Paleocene) revisited: settling chronologies of sedimentary records across the Atlantic and Pacific Oceans. Earth and Planetary Science Letters 405, 119–131.

Farouk, S., Jain, S., Ahmad, F., Abu-Alam, T., Al-Kahtany, K., El Agroudy, I.S., Bazeen, Y.S., Shaker, F., 2023. Multiproxy analyses of paleoenvironmental and paleoceanographic changes during the Danian-Selandian in East Central Sinai: an integrated stable isotope and planktic foraminiferal data. Frontiers in Earth Science 11, 1158991.

Fendley, I.M., Sprain, C.J., Renne, P.R., Arenillas, I., Arz, J.A., Gilabert, V., Self, S., Vanderkluysen, L., Pande, K., Smit, J., Mittal, T., 2020. No Cretaceous-Paleogene boundary in exposed Rajahmundry Traps: a refined chronology of the longest Deccan lava flows from $^{40}Ar/^{39}Ar$ dates, magnetostratigraphy, and biostratigraphy. Geochemistry, Geophysics, Geosystems 21, e2020GC009149.

Font, E., Adatte, T., Andrade, M., Keller, G., Mbabi Bitchong, A., Carvallo, C., Ferreira, J., Diogo, Z., Mirão, J., 2018. Deccan volcanism induced high-stress environment during the Cretaceous–Paleogene transition at Zumaia, Spain: evidence from magnetic, mineralogical and biostratigraphic records. Earth and Planetary Science Letters 484, 53–66.

Font, E., Chen, J., Regelous, M., Regelous, A., Adatte, T., 2022. Volcanic origin of the mercury anomalies at the Cretaceous-Paleogene transition of Bidart, France. Geology 50, 142–146.

Galeotti, S., Moretti, M., Cappelli, C., Phillips, J., Lanci, L., Littler, K., Monechi, S., Petrizzo, M.R., Silva, I.P., Zachos, J.C., 2015. The Bottaccione section at Gubbio, central Italy: a classical Paleocene Tethyan setting revisited. Newsletters on Stratigraphy 48, 325–339.

Gerstel, J., Thunell, R.C., Zachos, J.C., Arthur, M.A., 1986. The Cretaceous/Tertiary Boundary event in the North Pacific: planktonic foraminiferal results from Deep Sea Drilling Project Site 577, Shatsky Rise. Paleoceanography 1, 97–117.

Gilabert, V., Arenillas, I., Arz, J.A., Batenburg, S.J., Robinson, S.A., 2021a. Multiproxy analysis of paleoenvironmental, paleoclimatic and paleoceanographic changes during the early Danian in the Caravaca section (Spain). Palaeogeography, Palaeoclimatology, Palaeoecology 576, 110513.

Gilabert, V., Arz, J.A., Arenillas, I., Robinson, S.A., Ferrer, D., 2021b. Influence of the Latest Maastrichtian Warming Event on planktic foraminiferal assemblages and ocean carbonate saturation at Caravaca, Spain. Cretaceous Research 125, 104844.

Gilabert, V., Batenburg, S.J., Arenillas, I., Arz, J.A., 2022. Contribution of orbital forcing and Deccan volcanism to global climatic and biotic changes across the Cretaceous-Paleogene boundary at Zumaia, Spain. Geology 50, 21–25.

Gradstein, F.M., Ogg, J.G., Schmitz, M.D., Ogg, G.M., 2020. The Geologic Time Scale 2020. Elsevier, Amsterdam.

Grasby, S.E., Them, T.R., Chen, Z., Yin, R., Ardakani, O.H., 2019. Mercury as a proxy for volcanic emissions in the geologic record. Earth-Science Reviews 196, 102880.

Henehan, M.J., Ridgwell, A., Thomas, E., Zhang, S., Alegret, L., Schmidt, D.N., Rae, J.W. B., Witts, J.D., Landman, N.H., Greene, S.E., Huber, B.T., Super, J.R., Planavsky, N.J., Hull, P.M., 2019. Rapid ocean acidification and protracted Earth system recovery followed the end-Cretaceous Chicxulub impact. Proceedings of the National Academy of Sciences 116, 22500–22504.

Hull, P.M., Bornemann, A., Penman, D.E., Henehan, M.J., Norris, R.D., Wilson, P.A., Blum, P., Alegret, L., Batenburg, S.J., Bown, P.R., Bralower, T.J., Cournede, C., Deutsch, A., Donner, B., Friedrich, O., Jehle, S., Kim, H., Kroon, D., Lippert, P.C., Loroch, D., Moebius, I., Moriya, K., Peppe, D.J., Ravizza, G.E., Röhl, U., Schueth, J. D., Sepúlveda, J., Sexton, P.F., Sibert, E.C., Sliwínska, K.K., Summons, R.E., Thomas, E., Westerhold, T., Whiteside, J.H., Yamaguchi, T., Zachos, J.C., 2020. On impact and volcanism across the Cretaceous-Paleogene boundary. Science 367, 266–272.

Hull, P.M., Norris, R.D., Bralower, T.J., Schueth, J.D., 2011. A role for chance in marine recovery from the end-Cretaceous extinction. Nature Geosciences 4, 856–860.

Jiang, S., Bralower, T.J., Patzkowsky, M.E., Kump, L.R., Schueth, J.D., 2010. Geographic controls on nannoplankton extinction across the Cretaceous/Palaeogene boundary. Nature Geoscience 3, 280–285.

Jones, H.L., Lowery, C.M., Bralower, T.J., 2019. Delayed calcareous nannoplankton boom-bust successions in the earliest Paleocene Chicxulub (Mexico) impact crater. Geology 47, 753–756.

Jones, H.L., Westerhold, T., Birch, H., Hull, P., Negra, M.H., Röhl, U., Sepúlveda, J., Vellekoop, J., Whiteside, J.H., Alegret, L., Henehan, M., Robinson, L., van Dijk, J., Bralower, T., 2023. Stratigraphy of the Cretaceous/Paleogene (K/Pg) boundary at the Global Stratotype Section and Point (GSSP) in El Kef, Tunisia: new insights from the El Kef Coring Project. Bulletin of the Geological Society of America 135, 2451–2477.

Jouini, A., Paris, G., Caro, G., Bartolini, A., Gardin, S., 2023. Constraining oceanic carbonate chemistry evolution during the Cretaceous-Paleogene transition: combined benthic and planktonic calcium isotope records from the equatorial Pacific Ocean. Earth and Planetary Science Letters 619, 118305.

Keller, G., 2008. Cretaceous climate, volcanism, impacts, and biotic effects. Cretaceous Research 29, 754–771.

Keller, G., Lindinger, M., 1989. Stable isotope, TOC and $CaCO_3$ record across the Cretaceous/Tertiary boundary at El Kef, Tunisia. Palaeogeography, Palaeoclimatology, Palaeoecology 73, 243–265.

Keller, G., Mateo, P., Monkenbusch, J., Thibault, N., Punekar, J., Spangenberg, J.E., Abramovich, S., Ashckenazi-Polivoda, S., Schoene, B., Eddy, M.P., Samperton, K. M., Khadri, S.F.R., Adatte, T., 2020. Mercury linked to Deccan Traps volcanism, climate change and the end-Cretaceous mass extinction. Global and Planetary Change 194, 103312.

Krahl, G., Arenillas, I., Gilabert, V., Kochhann, K.G.D., Bom, M.H.H., Fauth, G., Arz, J.A., 2023. Impact of early Danian environmental perturbations on mid-latitude planktic foraminiferal assemblages from the ODP-1262 (South Atlantic Ocean). Newsletters on Stratigraphy 56, 377–403.

Krahl, G., Bom, M.H.H., Kochhann, K.G.D., Souza, L.V., Savian, J.F., Fauth, G., 2020. Environmental changes occurred during the Early Danian at the Rio Grande Rise, South Atlantic Ocean. Global and Planetary Change 191, 103197.

Kroon, D., Zachos, J.C., 2007. Leg 208 synthesis: Cenozoic climate cycles and excursions (Leg 208 Scientific Party). In: Kroon, D., Zachos, J.C., Richter, C. (Eds.), Proceedings of the Ocean Drilling Program, Scientific Results. Ocean Drilling Program, College Station, Texas, pp. 1–55.

Laskar, J., Gastineau, M., Delisle, J.-B., Farrés, A., Fienga, A., 2011. Strong chaos induced by close encounters with Ceres and Vesta. Astronomy and Astrophysics 532, 4.

Li, L., Keller, G., 1998. Maastrichtian climate, productivity and faunal turnovers in planktic foraminifera in South Atlantic DSDP sites 525A and 21. Marine Micropaleontology 33, 55–86.

Lowery, C.M., Jones, H.L., Bralower, T.J., Cruz, L.P., Gebhardt, C., Whalen, M.T., Chenot, E., Smit, J., Phillips, M.P., Choumiline, K., Arenillas, I., Arz, J.A., Garcia, F., Ferrand, M., Gulick, S.S.P., 2021. Early paleocene paleoceanography and export productivity in the chicxulub crater. Paleoceanography and Paleoclimatology 36, e2021PA004241.

Nauter-Alves, A., Dunkley-Jones, T., Bruno, M.D.R., De Lira Mota, M.A., Cachão, M., Krahl, G., Fauth, G., 2023. Biotic turnover and carbon cycle dynamics in the early Danian event (Dan-C2): new insights from Blake Nose, North Atlantic. Global and Planetary Change 221, 104046.

Percival, L.M.E., Jenkyns, H.C., Mather, T.A., Dickson, A.J., Batenburg, S.J., Ruhl, M., Hesselbo, S.P., Barclay, R., Jarvis, I., Robinson, S.A., Robinson, S.A., Woelders, L., 2018. Does large igneous province volcanism always perturb the mercury cycle? Comparing the records of Oceanic Anoxic Event 2 and the end-Cretaceous to other Mesozoic events. American Journal of Science 318, 799–860.

Pickersgill, A.E., Mark, D.F., Lee, M.R., Kelley, S.P., Jolley, D.W., 2021. The Boltysh impact structure: an early Danian impact event during recovery from the K-Pg mass extinction. Science Advances 7, 1–10.

Quillévéré, F., Norris, R.D., Kroon, D., Wilson, P.A., 2008. Transient ocean warming and shifts in carbon reservoirs during the early Danian. Earth and Planetary Science Letters 265, 600–615.

Regelous, A., Ćorić, S., Regelous, M., Teipel, U., 2022. Geochemical anomalies caused by meteorite impact and volcanism at the Cretaceous-Paleogene boundary, Wasserfallgraben (Lattengebirge, Germany). Cretaceous Research 140, 105306.

Renne, P.R., Deino, A.L., Hilgen, F.J., Kuiper, K.F., Mark, D.F., Mitchell, W.S., Morgan, L. E., Mundil, R., Smit, J., 2013. Time scales of critical events around the Cretaceous-Paleogene boundary. Science 339, 684–687.

Renne, P.R., Sprain, C.J., Richards, M.A., Self, S., Vanderkluysen, L., Pande, K., 2015. State shift in Deccan volcanism at the Cretaceous-Paleogene boundary, possibly induced by impact. Science 350, 76–78.

Richards, M.A., Alvarez, W., Self, S., Karlstrom, L., Renne, P.R., Manga, M., Sprain, C.J., Smit, J., Vanderkluysen, L., Gibson, S.A., 2015. Triggering of the largest Deccan eruptions by the Chicxulub impact. Geological Society of America Bulletin 127, 1507–1520.

Schoene, B., Eddy, M.P., Samperton, K.M., Keller, C.B., Keller, G., Adatte, T., Khadri, S. F.R., 2019. U-Pb constraints on pulsed eruption of the Deccan Traps across the end-Cretaceous mass extinction. Science 363, 862–866.

Schulte, P., Alegret, L., Arenillas, I., Arz, J.A., Barton, P.J., Bown, P.R., Bralower, T.J., Christeson, G.L., Claeys, P., Cockell, C.S., Collins, G.S., Deutsch, A., Goldin, T.J., Goto, K., Grajales-Nishimura, J.M., Grieve, R.A.F., Gulick, S.P.S., Johnson, K.R., Kiessling, W., Koeberl, C., Kring, D.A., MacLeod, K.G., Matsui, T., Melosh, J., Montanari, A., Morgan, J.V., Neal, C.R., Nichols, D.J., Norris, R.D., Pierazzo, E., Ravizza, G., Rebolledo-Vieyra, M., Reimold, W.U., Robin, E., Salge, T., Speijer, R.P., Sweet, A.R., Urrutia-Fucugauchi, J., Vajda, V., Whalen, M.T., Willumsen, P.S., 2010. The Chicxulub asteroid impact and mass extinction at the Cretaceous-Paleogene boundary. Science 327, 1214–1218.

Sepúlveda, J., Alegret, L., Thomas, E., Haddad, E., Cao, C., Summons, R.E., 2019. Stable isotope constraints on marine productivity across the Cretaceous-Paleogene mass extinction. Paleoceanography and Paleoclimatology 34, 1195–1217.

Sinnesael, M., De Vleeschouwer, D., Coccioni, R., Claeys, P., Frontalini, F., Jovane, L., Savian, J.F., Montanari, A., 2016. High-resolution multiproxy cyclostratigraphic analysis of environmental and climatic events across the Cretaceous-Paleogene boundary in the classic pelagic succession of Gubbio (Italy). Geological Society of America Special Papers 524, 115–137.

Smit, J., Koeberl, C., Claeys, P., Montanari, A., 2016. Mercury anomaly, Deccan volcanism, and the end-Cretaceous mass extinction: comment. Geology 44, e381.

Sprain, C.J., Renne, P.R., Clemens, W.A., Wilson, G.P., 2018. Calibration of chron C29r: new high-precision geochronologic and paleomagnetic constraints from the Hell Creek region, Montana. Geological Society of America Bulletin 130, 1615–1644.

Sprain, C.J., Renne, P.R., Vanderkluysen, L., Pande, K., Self, S., Mittal, T., 2019. The eruptive tempo of Deccan volcanism in relation to the Cretaceous-Paleogene boundary. Science 363, 866–870.

Swart, P.K., 2015. The geochemistry of carbonate diagenesis: the past, present and future. Sedimentology 62, 1233–1304.

Westerhold, T., Röhl, U., Donner, B., McCarren, H.K., Zachos, J.C., 2011. A complete high-resolution Paleocene benthic stable isotope record for the central Pacific (ODP-1209). Paleoceanography 26, 1–13.

Woelders, L., Vellekoop, J., Kroon, D., Smit, J., Casadío, S., Prámparo, M.B., Dinarès-Turell, J., Peterse, F., Sluijs, A., Lenaerts, J.T.M., Speijer, R.P., 2017. Latest Cretaceous climatic and environmental change in the South Atlantic region. Paleoceanography 32, 466–483.